PHENIX Calorimeter

L. Aphecetche [f] T.C. Awes [g] J. Banning [g] S. Bathe [e]
A. Bazilevsky [i] S. Belikov [b,h] S.T. Belyaev [c] C. Blume [e]
M. Bobrek [g] D. Bucher [e] V. Bumazhnov [h] H. Büsching [e]
S.Chernichenkov [h] V. Cianciolo [g] M. Cutshaw [g]
D.G. D'Enterria [f] S. Daniels [g] G. David [a] H. Delagrange [f]
A. Denisov [h] A. Durum [h] Y.V. Efremenko [g] M.S. Emery [g]
S.L. Fokin [c] S. Frank [g] Y. Goto [i] M. Grosse Perdekamp [i]
N. Heine [e] D.E. Hurst [g] V.V. Ikonnikov [c] M.S. Ippolitov [c]
G. Jackson [g] J.P. Jones [g] K.V. Karadjev [c] E. Kistenev [a]
C. Klein-Bösing [e] V. Kochetkov [h] Iou.A. Koutcheryaev [c]
V.A. Lebedev [c] V.I. Manko [c] G. Martinez [f] Y. Melnikov [h]
T. Moore [g] M. Musrock [g] S.A. Nikolaev [c] A.S. Nyanin [c]
V. Onuchin [h] T. Peitzmann [e] P. Pitukhin [h] F. Plasil [g]
K.F. Read [g] K. Reygers [e] R. Santo [e] Y. Schutz [f] V. Semenov [h]
V. Shelikhov [h] Iou.G. Sibiriak [c] M. Simpson [g] D.C. Smith [g]
M. Smith [g] A. Soldatov [h] P.W. Stankus [g] J. Stewering [e]
S.P. Stoll [a] H. Torii [d] A.A. Tsvetkov [c] N. Tyurin [h] A. Usachev [h]
A.A. Vasiliev [c] W. Verhoeven [e] A.A. Vinogradov [c] M.A. Volkov [c]
J.W. Walker [g] S.N. White [a] A.L. Wintenberg [g] C.L. Woody [a]
G.R. Young [g] I.E. Yushmanov [c]

(The PHENIX Collaboration)

[a] *Brookhaven National Laboratory, Upton, NY 11973-5000, USA*

[b] *Iowa State University, Ames, IA 50011, USA*

[c] *Russian Research Center "Kurchatov Institute", RU-123182, Moscow, Russia*

[d] *Kyoto University, Kyoto 606, Japan*

[e] *University of Münster, D-411980, Münster, Germany*

[f] *SUBATECH (Ecole des Mines de Nantes, IN2P3/CRNS, Universite de Nantes) BP 20722-44307, Nantes-cedex 3, France*

[g] *Oak Ridge National Laboratory, Oak Ridge, TN 37831, USA*

[h] *Institute for High Energy Physics (IHEP), Protvino, Russia*

[i] *RIKEN BNL Research Center, Brookhaven National Laboratory, Upton, NY 11973-5000, USA*

The PHENIX Electromagnetic Calorimeter (EMCal) is used to measure the spatial position and energy of electrons and photons produced in heavy ion collisions. It covers the full central spectrometer acceptance of $70^\circ \leq \theta \leq 110^\circ$ with two walls, each subtending 90° in azimuth. One wall comprises four sectors of a Pb-scintillator sampling calorimeter and the other has two sectors of Pb-scintillator and two of a Pb-glass Cherenkov calorimeter. Both detectors have very good energy, spatial and timing resolution, while the Pb-scintillator excels in timing and the Pb-glass in energy measurements. Also, having two detectors with different systematics increases the confidence level of the physics results. Design and operational parameters of the Pb-scintillator, Pb-glass and special readout electronics for EMCal are presented and running experience during the first year of data taking with PHENIX is discussed. Some examples of data taken during the first run are shown.

1 Introduction

The PHENIX detector [1] at the Relativistic Heavy Ion Collider is designed to measure the properties of nuclear matter at the highest temperatures and energy densities yet produced in terrestrial experiments and to search for new phenomena such as the quark-gluon plasma. The primary role of the Electromagnetic Calorimeter (EMCal) in PHENIX is to provide a measurement of the energies and spatial positions of photons and electrons produced in heavy ion collisions. It also plays a major role in particle identification and is an important part of the PHENIX trigger system. The EMCal system can trigger on rare events with high transverse momentum (p_T) photons and electrons. Its signals are incorporated in Level-1 triggers for high multiplicity or large total transverse energy (E_T) events. In addition the EMCal provides a good measurement of the *hadronic* energy produced at mid-rapidity and thus of the E_T produced in the reaction.

The EMCal system consists of a total of 24768 individual detector modules divided between the Pb-Scintillator calorimeter, which provides six sectors of azimuthal coverage and the Pb-glass calorimeter comprised of two sectors. Both subdetectors are read out with photomultipliers and have good energy resolution and intrinsic timing characteristics but their design is quite different and they will be described separately. A description of special EMCal front-end electronics is also given. The position of the EMCal relative to the rest of the PHENIX detector is illustrated in Fig. 2 in the article entitled “PHENIX Detector Overview” in this volume [1] and a view in a cut through the collision vertex is shown in Fig. 1 in the article entitled “PHENIX Central Arm Tracking Detectors” also in this volume [2].

The properties of the Pb-scintillator and Pb-glass calorimeters are very different and they have different strengths and weaknesses. The Pb-scintillator is a sampling calorimeter while the Pb-glass is a Cherenkov detector. For the two detectors the granularity, energy resolution, linearity, response to hadrons, timing properties and shower shape at normal and non-normal impact on the face of the tower differ significantly. For example the Pb-glass has the best granularity and energy resolution but the Pb-scintillator has the best linearity and timing and the response to hadrons is better understood. Due to this the data analysis, particle identification cuts and the resulting systematic errors are also different and will be discussed in separate sections. Nevertheless choosing two different technologies was a deliberate decision by PHENIX which has the advantage of producing independent cross checks of results within the same experiment.

2 Lead-Scintillator Calorimeter

The Pb-scintillator electromagnetic calorimeter is a shashlik type sampling calorimeter made of alternating tiles of Pb and scintillator consisting of 15552 individual towers and covering an area of approximately 48 m^2. The basic building block is a module consisting of four (optically isolated) towers which are read out individually. The modules were manufactured in Russia and subjected to quality control procedures designed to achieve consistent large light yield in all towers ($\sim 12500 photons/GeV$). The PbSc calorimeter has a nominal energy resolution of $8.1\%/\sqrt{E}(GeV) \oplus 2.1\%$ and an intrinsic timing resolution better than 200 ps for electromagnetic showers [3]. A high precision calibration and monitoring system has been developed to achieve an absolute energy calibration better than 5% for day one operation at RHIC, and to maintain an overall long term gain stability of the order of 1%. Details of the two calorimeter types are given in sections 2 and 3 below and the front-end electronics for both are discussed in section 4.

2.1 Pb-Scintillator Calorimeter Design

2.1.1 Opto-Mechanical Design

Each Pb-scintillator tower contains 66 sampling cells consisting of alternating tiles of Pb and scintillator. The edges of the tiles are plated with Al. These cells are optically connected by 36 longitudinally penetrating wavelength shifting fibers for light collection. Light is read out by 30 mm FEU115M phototubes at the back of the towers. Four towers are mechanically grouped together into a single structural entity called a module as shown in Fig. 1. Thirty six modules are attached to a backbone and held together by welded stainless steel skins on the outside to form a rigid structure called a supermodule. Eighteen supermodules make a "sector", a $2 \times 4\ m^2$ plane with its own rigid steel frame. Details of the design and methods of construction of the Pb-scintillator modules have been given in an earlier publication [4]. All major Pb-scintillator design parameters are listed in Table 1. The scintillating plastic contains an organic scintillator p-bis[2-(5-Phenyloxazolyl)]-benzene (POPOP) and a fluorescent additive p-Terphenyl (PT).

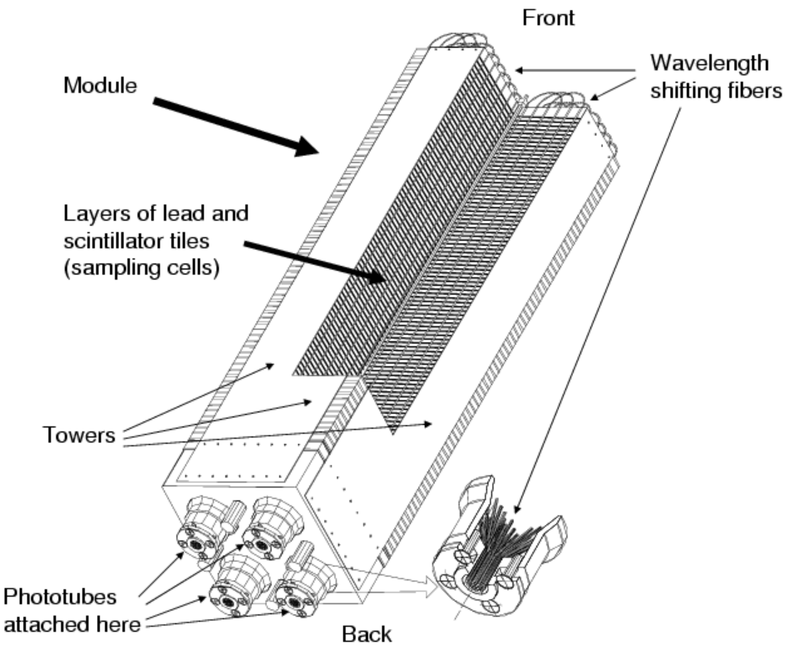

Fig. 1. Interior view of a Pb-scintillator calorimeter module showing a stack of scintillator and lead plates, wavelength shifting fiber readout and leaky fiber inserted in the central hole.

2.1.2 Monitoring System Design

The calibration and monitoring system is based on a UV laser which supplies light to the calorimeter through a series of optical splitters and fibers. The block diagram of the monitoring system is shown schematically in Fig. 2 [5].

Light from a high power YAG laser is initially split into six equal intensity beams using a set of partially reflecting mirrors. The beam from each mirror passes through a quartz lens and is focused to a point just in front of a quartz fiber which is used to transport the light over a distance of approximately 50 meters to one sector of the calorimeter. Optical splitters are used to distribute the light to each of the individual calorimeter modules. At the very

Table 1
Individual Pb-Scintillator Calorimeter Tower Parameters

Parameter	Value
Lateral Segmentation	$5.535 \times 5.535\ cm^2$
Active Sampling Cells	66
Scintillator	Polystyrene (1.5% PT / 0.01% POPOP), 0.4 cm
Absorber	Pb, 0.15 cm
Cell Thickness	0.56 cm (0.277 $X_\circ$)
Active Depth	37.5 cm
Radiation Length	18
Nuclear Interaction Length	0.85
WLS Fiber	BCF-99-29a, 0.1 cm
WLS Fibers per Tower	36
PMT Type	FEU115M, MELS, Russia, 3.0 cm
Photocathode	Sb-K-Na-Cs
Luminous Sensitivity	$\geq 80\ \mu$a/lm
Rise Time (20%–80%)	≤ 5 ns

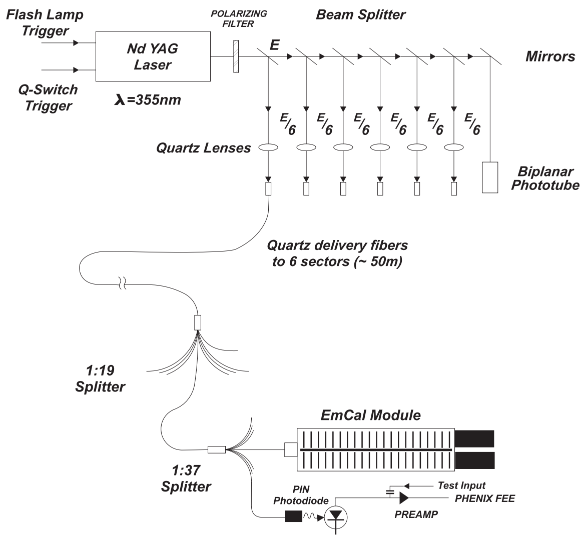

Fig. 2. Laser light distribution and monitoring system

last stage the light is injected into a 38 cm long, 2 mm diameter plastic fiber that penetrates the center of the module (there is a small gap in the optical isolation of the towers). This "leaky fiber" is grated such that light exits along its length simulating the depth profile of a 1 GeV electromagnetic shower in the four surrounding towers. The overall efficiency to produce one photoelectron in each of the 15592 towers from the primary photons of the laser is of the order of 4×10^{-12}. Given that the calorimeter has an intrinsic light output of $\sim$ 1500 photoelectrons per GeV, this leads to an energy requirement of $\sim$ 0.2 mJ per pulse from the YAG laser to deliver 1 GeV of equivalent energy into each tower.

2.2 Energy Calibration and Gain Monitoring

The initial calibration coefficients were established as follows. The calorimeter response to cosmic ray muons penetrating the supermodule in a direction nearly orthogonal to the tower axis was recorded along with the response to laser pulses. The absolute energy scale for muons was in turn established by test-beam measurements using electrons of known energy [4]. During the same test-beam exposure the response to relativistic (1 GeV/c $\pi^{\pm}$) charged particles which traverse the calorimeter was characterized by the minimum ionizing peak (MIP).

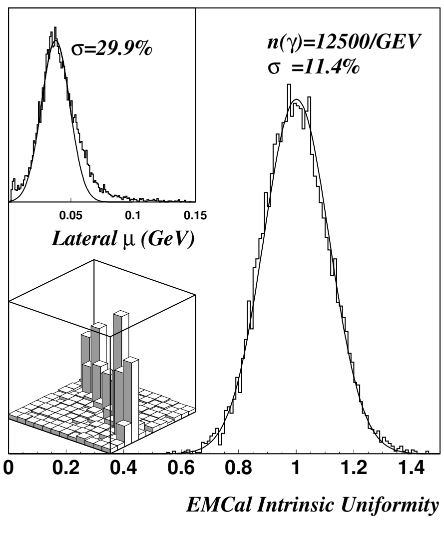

Fig. 3. Light yield uniformity in the Pb-scintillator calorimeter. The energy distribution in the towers exposed to laterally penetrating cosmic muons is shown in the top left insert and a lego plot of energies deposited in the towers by laterally penetrating cosmic muons is shown at the bottom left.

A lego plot of the energies deposited by a laterally penetrating muon in neighboring towers of a supermodule is shown in the bottom left plot of Fig. 3. The top left plot in the same figure shows the energy spectrum in one tower exposed to laterally penetrating muons. The MIP peak corresponds to 38 MeV in this case (270 MeV for longitudinally traversing particles) and has a nearly gaussian shape with $\sigma(E)/E$ ~30%. On average the EMCal towers produce

12500 photons per GeV of deposited electromagnetic energy. The distribution of the light yield (normalized to an average value) for ∼8000 towers is also shown in the same figure. Both the precalibration and original light yield measurements were performed with a "standard set" of phototubes, whose quantum efficiencies and gains differ from the actual tubes used in the final assembly. The laser monitoring system was used to transfer the initial calibration into the RHIC operational environment. After renormalization, the dispersion in the actual response of each tower with respect to the original muon calibration was only 2.3%. This residual dispersion is due mainly to the nonuniformities in the quantum efficiencies of the phototubes over the active photocathode area. The implemented scheme for calorimeter precalibration and further monitoring ensured a very low uncertainty in the absolute energy scale for day one operation at RHIC, well below the design goal of 5%.

2.3 Energy and Position Measurements with the Test Beam

The Pb-scintillator calorimeter went through a rather extensive sequence of preconstruction tests in the particle beams from U70 (IHEP, Protvino), from the AGS (BNL) and finally from the SPS (CERN). The correlation plot between the incident beam energy and the energy measured in the calorimeter is presented in Fig. 4. Data are normalized to 1 GeV. The finite light attenuation length (100 cm) in the WS fibers is a major contributor to the response nonuniformities at the low end of the energy scale, although this effect is mitigated by the fact that each fiber is looped back (see Fig. 1), and the light collected always has a short and a long path to the phototube. Other contributors at low energies are coarse sampling [6] and energy leakage at the front face [7]. At high momenta the "positive" effect of the light attenuation in the fibers is overcompensated by the "negative" effect of energy leakage from the back of the calorimeter. The resulting nonlinearity is about a factor of 2 lower than what one would expect from the effect of light attenuation alone.

The calorimeter energy resolution (corrected for the noise contribution) is shown in Fig. 5. The resolution is given by

$$8.1\%\sqrt{E(GeV)} \oplus 2.1\% \qquad (1)$$

The 8.1% value for the stochastic term is close to the expected resolution from sampling as predicted by GEANT.

The main contributors to the constant term are intrinsic nonuniformities, in particular tower boundaries, hot spots at fiber positions and shower depth fluctuations. (The latter are responsible for the variations in the amount of

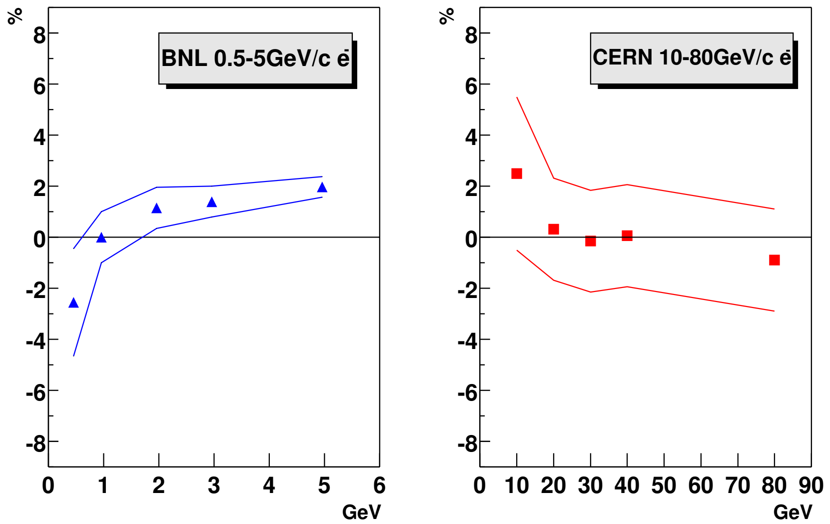

Fig. 4. Pb-scintillator EMCal energy linearity measured in beam tests at BNL (left) and CERN (right). The residual (calorimeter measured energy less the beam energy, divided by the beam energy) is for the 5×5 tower energy sum. The solid lines show total systematic uncertainties in the analysis.

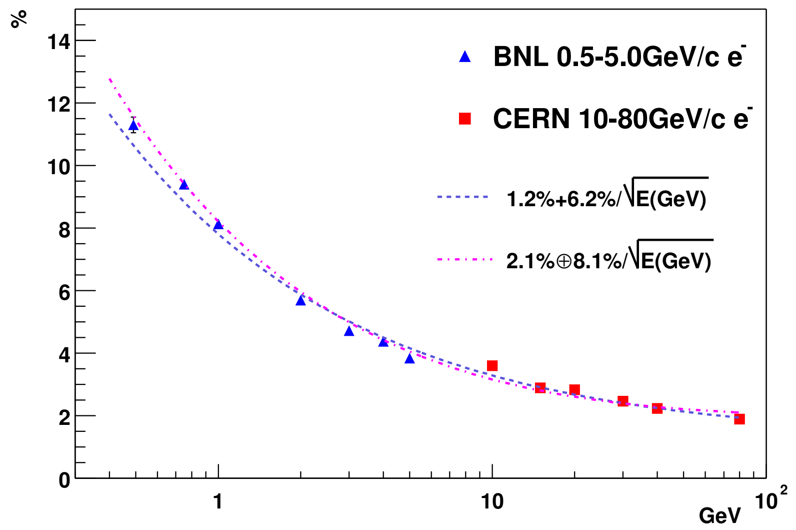

Fig. 5. Pb-scintillator EMCal energy resolution obtained by beam tests at CERN and BNL. The dashed line shows a fit to the linear formula $\sigma_(E)/E = 1.2\% + 6.2\%/\sqrt(E(GeV))$. The dashed-dotted line shows the fit to the quadratic formula $\sigma_(E)/E = 2.1\% \oplus 8.1\%/\sqrt(E(GeV))$.

the light seen and in the energy leaking from the calorimeter via the front and back surfaces).

In order to study the lateral response nonuniformity, different areas of the calorimeter were exposed to 1 GeV/c electrons whose impact point was measured to better than 3 mm. The response variation was ±2.5%. The 8% loss in the calorimeter response from particles hitting the corner of the towers is the main factor in the relatively large constant term in the expression for the energy resolution.

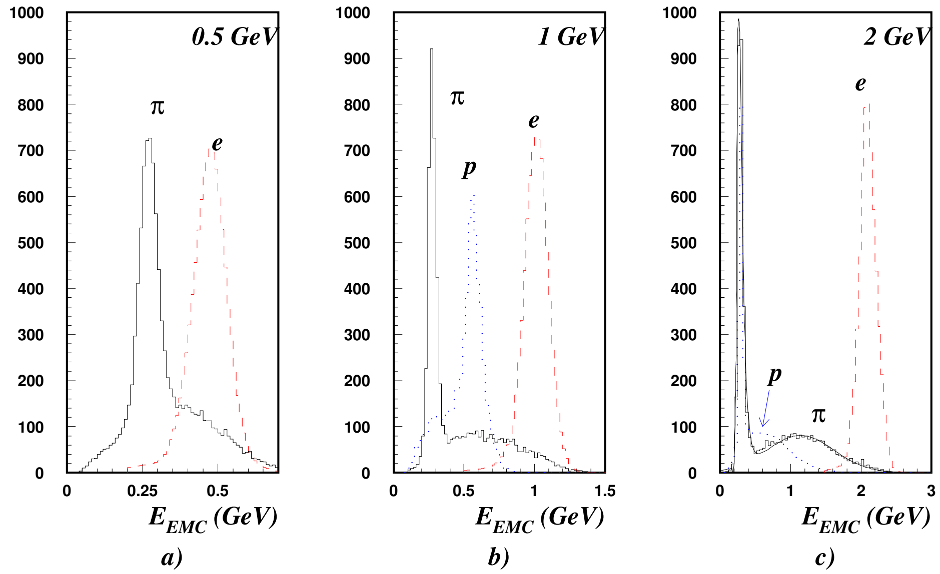

Fig. 6. The energy spectra measured in the PHENIX EMCal when exposed to electrons, pions and protons of 0.5, 1 and 2 GeV/c.

The depth of the Pb-scintillator electromagnetic calorimeter measured in units of nuclear interaction length at normal incidence is 0.85 L_{abs}. Lineshapes for protons and pions are shown on Fig. 6 along with electrons of the same momentum for comparison.

Both simulated (GEANT) and experimental data (taken at different impact angles) show that the measured shower shape (the projection onto the front face of the calorimeter) becomes skewed for non-normal angles of incidence. The data also show a gradual spread of the shower core mainly related to the longitudinal shower fluctuations contributing to the observed width, which in turn depends on impact angle θ as

$$b(\theta) = b_0 \oplus a(E) \times \sin^2(\theta) \tag{2}$$

where $b_0 = 7.3$ mm is the average width of 1 GeV electromagnetic showers for $\theta = 0$ (orthogonal impact). At larger angles the contribution from longitudinal fluctuations becomes dominant and the position resolution degrades.

All available data on position resolution can be well described by the simple formula

$$\sigma_x(E,\theta) = \sigma_0(E) \oplus \Delta \times \sin(\theta) \tag{3}$$

where‘

$$\sigma_0(E) = 1.55 \oplus \frac{5.7}{\sqrt{E}}\ (mm), \qquad E(GeV) \tag{4}$$

is the position resolution for normal incidence and $\Delta \sim L_{rad}$.

2.4 Particle Identification with the Pb-Scintillator Calorimeter

2.4.1 Effect of Shower-Shape Measurements on Photon Identification and Hadron Rejection

Since electromagnetic and hadronic particles produce quite different patterns of energy sharing between calorimeter towers, second moments of the measured showers are often used to differentiate between them. However, in an earlier paper[8] we introduced a model which uses an analytical parametrization of the energy sharing and its fluctuations based upon measurements of identified electrons. The parameterization is used to compute $\chi^2 = \sum_i \frac{(E_i^{pred} - E_i^{meas})^2}{\sigma_i^2}$ where E_i^{meas} is the energy measured in tower i and E_i^{pred} is the predicted energy (using the parametrization and the actual measured impact point) for an electromagnetic particle of total energy $\sum_i E_i^{meas}$. This χ^2 value characterizes how “electromagnetic” a particular shower is and can be used to discriminate against hadrons. The important new feature of this model is that the fluctuations are also parameterized. Therefore, the resulting χ^2 distribution is close to the theoretical one and it is nearly independent of the energy or the impact angle of the electron. The χ^2 distributions for 2 GeV/c electrons and pions (with energy deposit above minimum ionization) are shown in Fig. 7. The arrow marks the χ^2 cut corresponding to 90% electron efficiency.

2.4.2 Time of Flight Measurements with the Calorimeter

Timing information from the calorimeter is used both for particle identification and in the pattern recognition to find overlapping showers. In particular, timing is the only tool to reject neutral baryons, and interacting antineutrons are a major contributor to clusters with energy $\sim 2GeV$. Also, large inconsistencies between the measured times in different towers of the same cluster often indicate the overlap of two particles with very different time of flight.

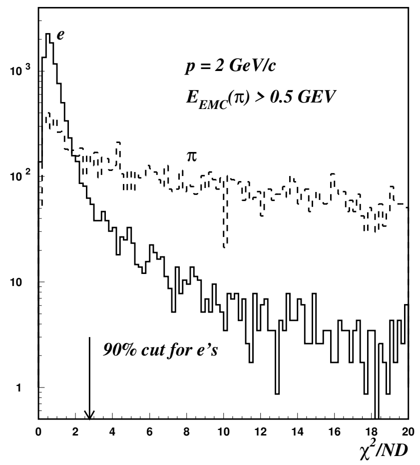

Fig. 7. χ^2 distribution for showers induced by 2 GeV/c electrons and pions in the Pb-scintillator calorimeter.

Slew corrected arrival times measured by exposing the calorimeter to electrons, pions and protons at 1 GeV/c momenta are shown in the top of Fig. 8. The distribution for electrons has a perfectly Gaussian shape with only a few events in the tails. Both the pion and proton distributions show the presence of tails and are slightly asymmetric. The timing resolution curves (stochastic term) plotted in Fig. 8 combine the points measured by exposing the calorimeter to the particles in the 0.3-1.0 GeV/c momentum range.

For energy deposits in the calorimeter $\geq 0.5 GeV$ the calorimeter timing resolution is nearly constant at $\sim 120ps$ for electrons and protons and $\sim 270ps$ for pions where shower fluctuations are the major contributor to the measured resolution. In general the data can be well fitted by the function:

$$\sigma_t = \sigma_{t0} + \sigma_{t1}/(E - E_{threshold}) \tag{5}$$

which includes a pole type divergence close to the threshold. Here σ_{t0} is an intrinsic timing resolution limit, presumably due to fluctuations in the localization of the shower, and σ_{t1} includes contributions due to photon statistics as well as pulse shape fluctuations.

2.5 Pb-Scintillator Performance During First Year Running

Photons are identified using time-of-flight and showershape (χ^2) cuts. The insert in Fig. 9 shows the $\gamma\gamma$ invariant mass distribution for minimum bias data of the same reaction.

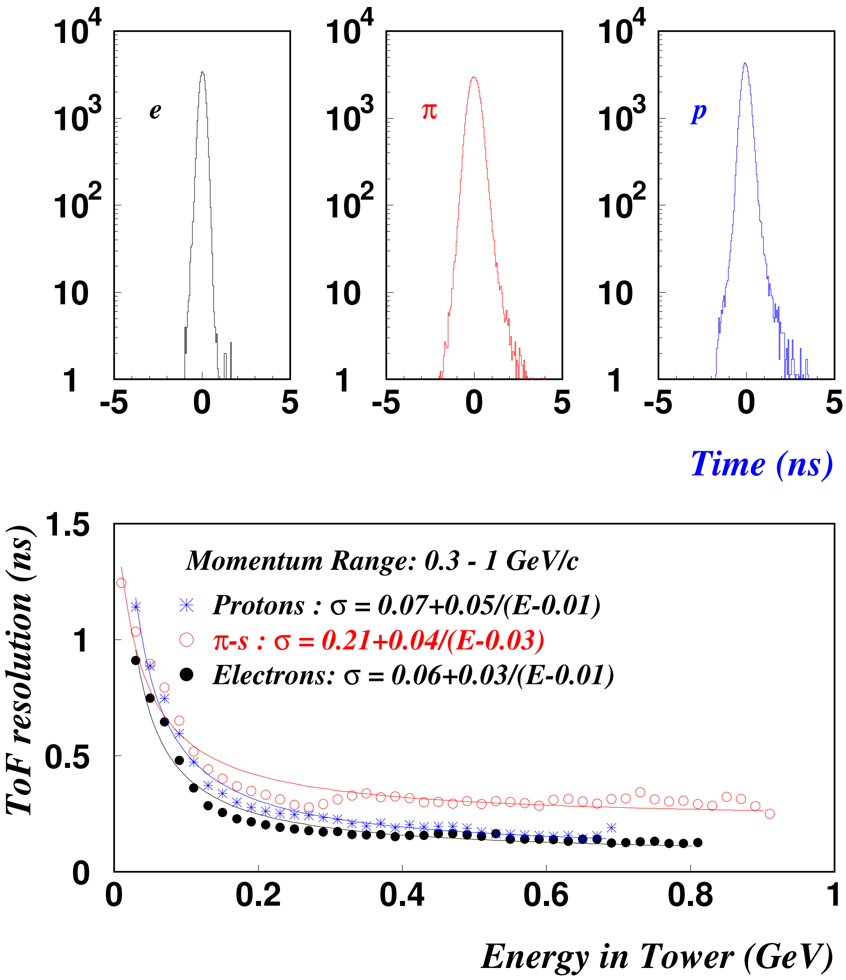

Fig. 8. Pb-scintillator timing resolution for different particles. Top: lineshape for 1 GeV/c electrons, pions and protons. Bottom: resolution in the momentum range 0.3-1.0 GeV/c

2.6 Summary for the Pb-Scintillator Calorimeter

We have designed and successfully constructed a 15552 channel electromagnetic calorimeter covering a total area of 48 m^2 using an approach optimized for industrial mass production. We relied heavily on industrial style quality control procedures to insure conformity to physics specifications. The calorimeter has a light yield of $\sim 12500 photons/GeV$ of electromagnetic energy. The calorimeter has energy and position resolutions ∼8% and ∼7 mm, respectively, for 1 GeV photons and electrons at normal incidence and gives a π^0 mass with resolution of ∼15 MeV. It has an excellent timing resolution of ∼100 ps for electromagnetic and ∼270 ps for hadronic showers which is nearly independent of the energy well above a threshold of about 10 MeV.

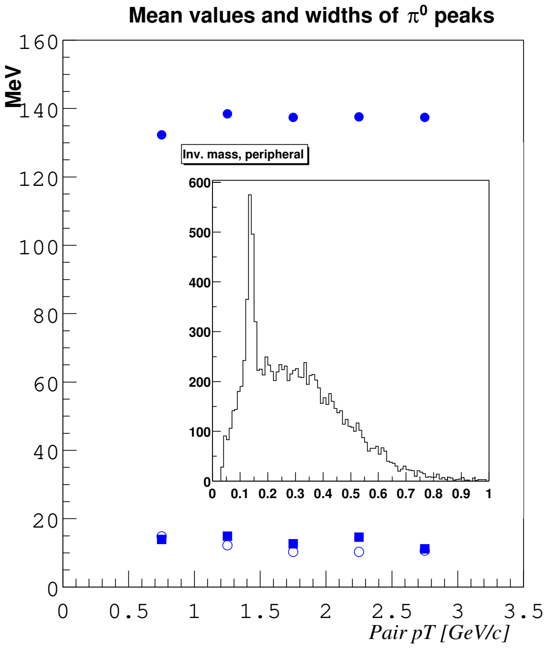

Fig. 9. Position and width of π^0 invariant mass peaks as a function of transverse momentum for peripheral Au-Au collisions at 130 GeV. The insert shows the $\gamma\gamma$ invariant mass distribution for minimum bias data of the same reaction. Closed squares show measured widths and open circles show simulated widths.

3 Lead-Glass Calorimeter

The Pb-glass calorimeter array comprises 9216 elements of a system previously used in CERN experiment WA98 [9]. It has a nominal energy resolution of $6\%/\sqrt{E}$(GeV) and an intrinsic timing resolution of better than 300 ps for electromagnetic showers above the minimum ionizing peak energy.

3.1 Pb-Glass Calorimeter Design

3.1.1 Mechanical Design

The Pb-glass calorimeter occupies the two lower sectors of the East Central arm of PHENIX. The PHENIX Time-of-Flight system [10] is located on the Pb-glass sectors. Each Pb-glass sector comprises 192 supermodules (SM) in an array of 16 Pb-glass SM wide by 12 SM high as shown in Fig.10. Each Pb-glass SM comprises 24 Pb-glass modules in a array of 6 Pb-glass modules wide by 4 modules high. Each Pb-glass module is 40 mm x 40 mm x 400 mm in size. The Pb-glass modules within a SM are individually wrapped with aluminized mylar and shrink tube and 24 modules are glued together with carbon fiber and epoxy resin to form a self-supporting SM with a shared calibration system (see Fig.10). Steel sheets 0.5 mm in thickness were used to house the phototubes and bases. The sheets were incorporated during the gluing process. An aluminized plastic foil on the front of the SM contains a hole for each Pb-glass module which allows entry for the LED light used for gain monitoring. A polystyrene reflective dome encloses the LED system on the front surface of the SM.

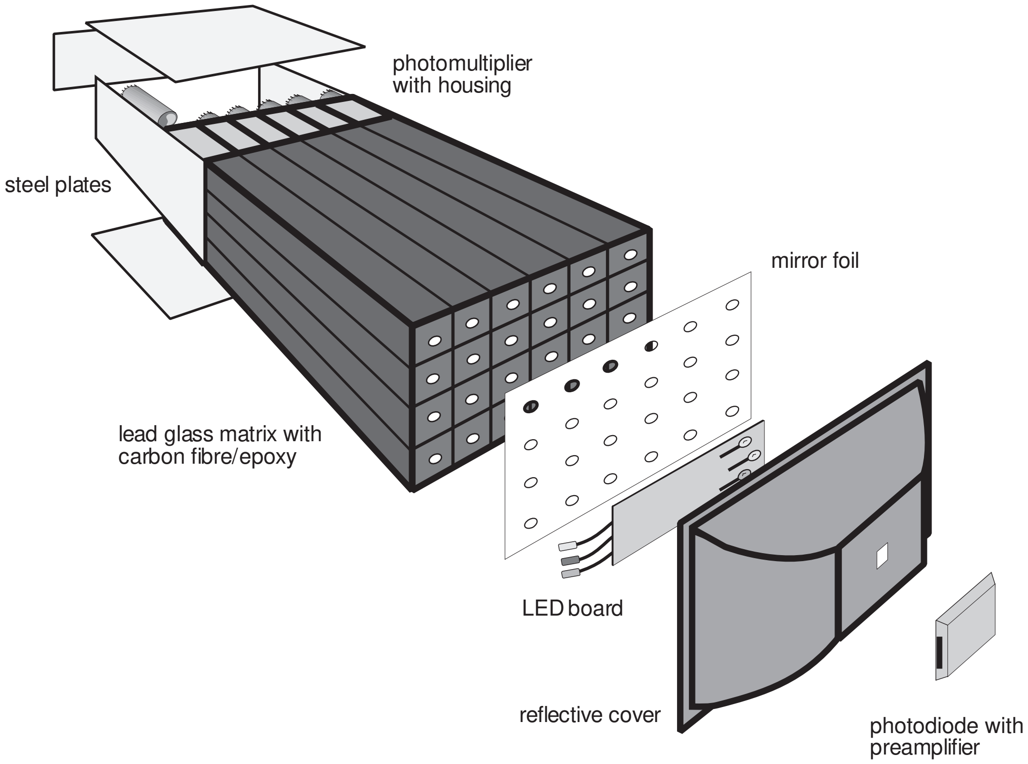

Fig. 10. Exploded view of a lead-glass detector supermodule.

Each Pb-glass module is read out with an FEU-84 photomultiplier. The high voltage for each photomultiplier is generated in a Cockcroft-Walton type photomultiplier base [11]. The high voltage for each module is individually controlled and read out with a custom VME based control system (HIVOC). Each HIVOC VME control module can control up to 2048 photomultipliers. Six PbGl SMs, 2 SM wide by 3 SM high, (144 individual Pb-glass modules) are read out with a single Front End Electronics (FEE) motherboard. The physical parameters of the Pb-glass detector system are summarized in Table 2.

3.1.2 Calibration and Monitoring System

Each Pb-glass supermodule (SM) has its own gain monitoring system based on a set of 3 LEDs which are viewed by all 24 Pb-glass modules within a SM [12]. Three LED's with different characteristics are employed. They are a fixed amplitude avalanche yellow LED with pulse shape most like real showers

Table 2
Lead-Glass Physical Parameters

Quantity	Value
Geometry:	384 Super Modules
Number of SM per Sector	192 (16 wide by 12 high)
Number of Modules per SM	24 (6 wide by 4 high)
Total Number of Modules	9216
Module Front Surface	4cm x 4cm
Module Length	40 cm (14.4 X_0)
Mylar Foil Thickness	12 micron
Shrink Tube Thickness	150 micron
Super Module Front Surface	24.6 ± 0.02cm x 16.4 ± 0.02cm
Pb-glass: Type	TF1
Pb-Oxide Content	51%
Density	3.85 g/cm^2
Weight per Module	2.46 kg
Index of Refraction	1.648
Total Internal Reflection Angle	36 degrees
Radiation Length	2.8 cm
Moliere Radius	3.68 cm
Interaction Length	38.0 cm
Critical Energy	16 MeV

together with a yellow and a blue LED which have amplitudes which may be varied. The absolute light yields of the LEDs of each SM are monitored by a photodiode which, together with preamp, is permanently attached to the SM. The photodiode-normalized avalanche yellow LED signal observed in each Pb-glass module was calibrated in GeV-equivalents using 10 GeV electrons in the CERN X1 beamline in the Fall 1993 and Spring 1994. The GeV equivalent of the avalanche yellow LEDs in individual modules ranged from 5 to 10 GeV. The Pb-glass calibration has been maintained to within approximately 10% for PHENIX using the LED/ photodiode system.

3.2 Test Beam Performance

The response of the Pb-glass electromagnetic calorimeter was studied extensively in test beams at the AGS(BNL) and SPS(CERN) to investigate the performance of the device with respect to energy, position and timing measurements and their variation with energy, position and angle of incidence.

3.2.1 Energy and Position Measurements

The measured energy resolution of e^+ showers versus the incident energy is shown in Fig. 11 for various angles of incidence on the calorimeter surface. The energy resolution results of Fig. 11 are shown with the fit parameterization

$$\frac{\sigma(E)}{E} = \frac{[5.9 \pm 0.1]\%}{\sqrt{E/\mathrm{GeV}}} \oplus [0.8 \pm 0.1]\%. \tag{6}$$

The measured position resolution can be fit with the parameterization

$$\sigma_x(E) = \frac{[8.4 \pm 0.3]\mathrm{mm}}{\sqrt{E/\mathrm{GeV}}} \oplus [0.2 \pm 0.1]\mathrm{mm}. \tag{7}$$

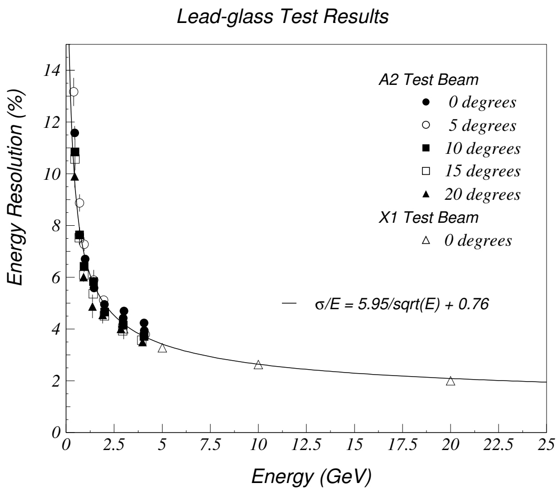

Fig. 11. PbGl energy resolution versus incident energy.

3.2.2 Particle Identification

The EMCal is designed to identify and measure the total energy of electrons and photons. The identification is assisted by the fact that hadrons typically do not shower or they deposit only a small fraction of their total energy in the calorimeter, since it is only about one interaction length in thickness (see Table 2). The hadron response of the PbGl calorimeter is further reduced by the fact that it observes only Čherenkov light. The Čherenkov threshold momenta (energies) for muons, pions and protons are 81, 106 and 715 MeV/c (27, 36 and 241 MeV), respectively. When the hadron momenta fall below these thresholds they will no longer produce Čherenkov light and their signal will be reduced. This is illustrated in Fig. 12 for 1 GeV/c protons and pions in comparison to electrons. The pions show a peak at around 460 MeV on a broad tail below the peak while the protons peak at around 80 MeV. At 4 GeV/c both protons and pions show a peak at about 540 MeV. At 500 MeV/c no significant signal is observed for protons and the pions show only a broad plateau from 0 to 500 MeV. At 150 MeV/c muons and pions deposit 55 and 25 MeV of apparent energy, respectively, when the electron signal is normalized to 150 MeV.

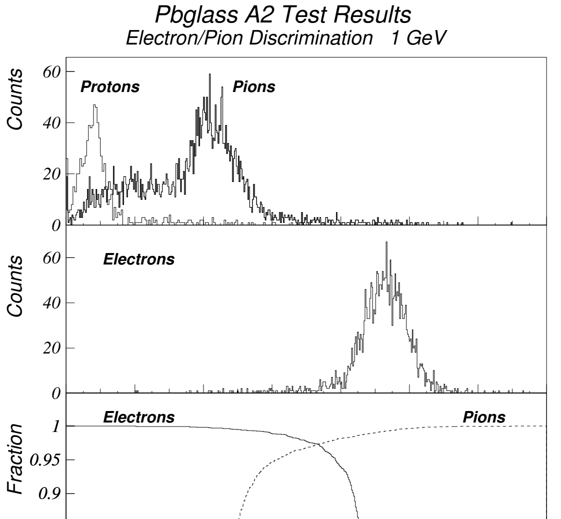

Fig. 12. Measured energy signal for protons, π^+ and e^+ of 1 GeV/c incident momentum. The lower panel shows the fraction of e^+ accepted or π^+ rejected for a varying threshold on the measured energy.

When the momentum of the charged hadron is measured in the PHENIX tracking system, the mismatch between the measured momentum and the deposited energy in the EMCal can be used to differentiate between hadrons

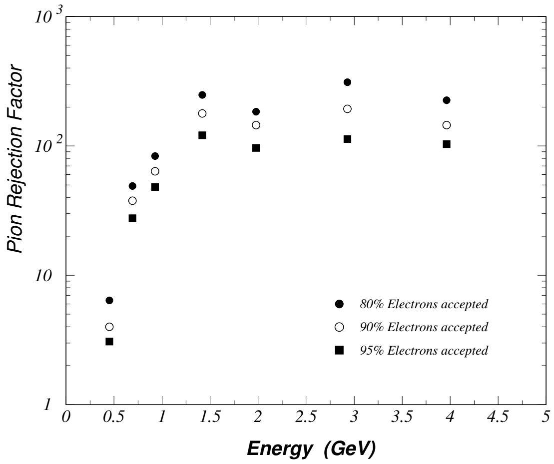

Fig. 13. Pion rejection factor versus incident energy.

and electrons. This is illustrated in the lower panel of Fig. 12. Using the fact that a 1 GeV/c track has been identified by the tracking system, the figure illustrates the fraction of electron tracks which would be accepted, as well as the fraction of pion tracks rejected, as a function of the required corresponding energy deposit in the Pb-glass. The pion rejection factors which can be obtained for various electron acceptance fractions as a function of the incident energy are shown in Fig. 13. An additional factor of about 2 can be obtained based on differences in the shower shape for hadrons which deposit the same energy as electromagnetic energy above about 1 GeV of energy deposit.

3.2.3 Time-of-Flight Measurements

The EMCal provides time-of-flight information to assist with hadron identification in the tracking system and to reject neutron and anti-neutron showers. The measured time-of-flight resolution as a function of the energy deposited in a single Pb-glass module is shown in Fig. 14 for electrons of various incident energies and pions of 1 GeV/c. The timing resolution can be parameterized in the form

$$\sigma_t(E_{Dep.}) = \frac{3.75\text{ns}}{\sqrt{500 \cdot E_{Dep.}/\text{GeV}}} \oplus 0.075\text{ns}. \tag{8}$$

The intrinsic timing resolution is seen to be similar for electromagnetic showers and decreasing with the increasing energy deposit according to the light produced (about 500 photoelectrons per GeV). The resolution falls below 200 ps in the upper range of momenta of interest to PHENIX. However, the use of the timing information from the PbGl is complicated by the fact that the arrival time of hadrons or hadron showers which pass through the PbGl (those which deposit more than about 500 MeV) have apparent arrival times which are about 800 ps faster than an electron of the same momentum. This is due to light from the faster transit time of the hadron to the rear of the lead-glass module compared to that of the Čherenkov light from the electromagnetic shower produced near the front of the module.

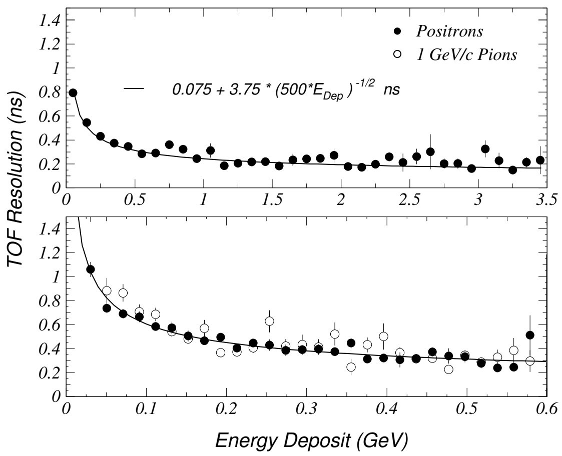

Fig. 14. Pb-glass timing resolution versus energy deposit in a single module for positrons of incident momenta 0.5, 0.75, 1.0, 1.5, 2,3 and 4.0 GeV/c and for 1.0 GeV/c pions.

3.3 Pb-Glass Calorimeter Performance in PHENIX

One full sector of the Pb-glass calorimeter was fully instrumented for the first PHENIX run period at RHIC with Au beams. An example of the performance is shown in Fig. 15 where the π^0 peak is observed in the two photon invariant mass distribution. The result is shown for peripheral Au-Au collisions at $\sqrt{s}$= 130 GeV per nucleon for photon pair transverse momentum in the range of 1.5-2.0 GeV/c.

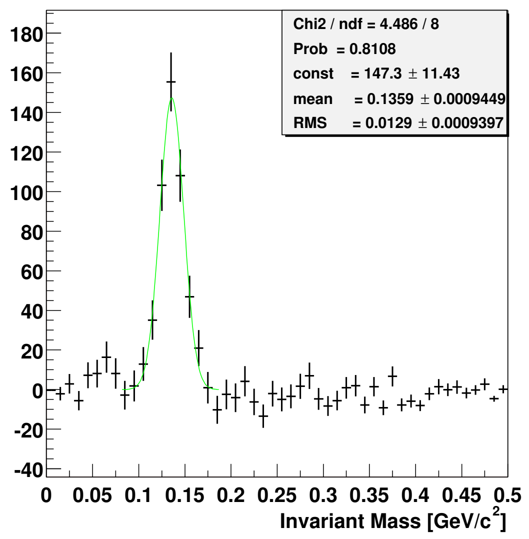

Fig. 15. The two photon invariant mass distribution after subtraction of the combinatorial pair background. The result is shown for peripheral Au-Au collisions at $\sqrt{s}$=130 GeV per nucleon for photon pair transverse momentum in the range of 1.5-2.0 GeV/c.

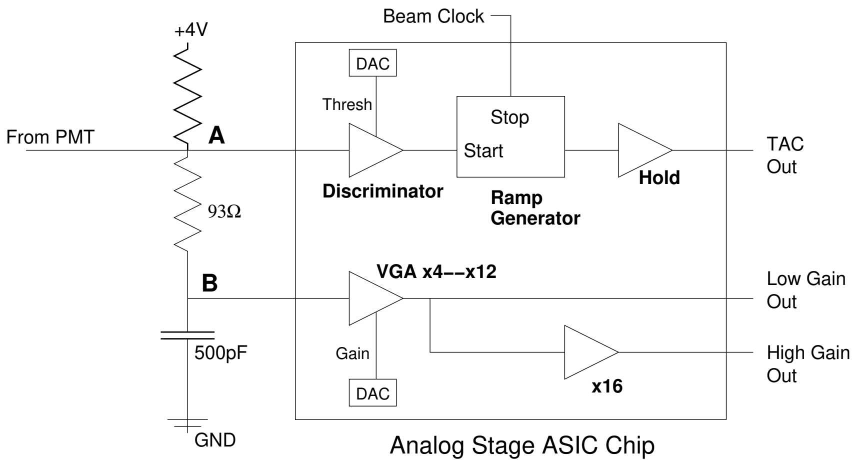

Fig. 16. Block diagram of the energy and timing measurement circuits.

4 Calorimeter Front-End Electronics

The readout electronics for the EMCal system conform to the general PHENIX Front-End Electronics (FEE) scheme [13] which includes periodic sampling synchronous with the RHIC RF clock and pipelined, deadtime-less conversion and readout. This section describes those features unique to the EMCal readout electronics and the way in which they satisfy the needs of the physics measurements made with the EMCal detector. Analog processing, digital processing and triggering are discussed below in sections 4.1, 4.2 and 4.3, respectively.

4.1 Analog Processing

On every event, for either physics or calibration data, each EMCal PMT emits a negative current pulse and each of these is processed by a chain as shown in Fig. 16. The salient features of the chain are discussed below.

There is no preamp or shaping stage other than passive integration. The 93 ohm resistor terminates the signal line from the PMT so the voltage profile at point A in Fig. 16 simply follows the current profile from the PMT which is a pulse with a $\leq$ 5 ns rise time. The charge is collected onto the 500 pF capacitor so the voltage profile at point B in Fig. 16 follows the integral of the current. The current pulse is a step function with a $\sim$100 ns rise time. The large resistor sets the quiescent voltage at this stage to +4 V to allow for negative-going pulses.

The fast voltage pulse discussed above is the "timing signal" that is used to measure the arrival time of the EM shower in the detector. During the pulse integration process a voltage step function is generated whose height is proportional to the total charge collected and thus the energy.collected during the time window of the event. All of the remaining analog processing stages up to ADC conversion are carried out within an ASIC [14] chip, as illustrated in Fig. 16. This chip was custom designed for the EMCal system. Each of these ASIC chips services four PMT channels and also contains the circuitry for the fast trigger function which is described below.

In the arrival time measurement the voltage pulse is discriminated, either in a leading-edge mode or a constant-fraction mode. The choice of mode, as well as the threshold voltages, are remotely selected *in situ* via ARCNet [13] which is the system used for monitoring and slow control of the PHENIX FEM's The discriminator firing starts a voltage ramp generator. The ramp is stopped on the next edge of the RHIC clock providing a *common-stop mode* TAC for each channel. After stopping the ramp voltage is held for two clock cycles where it settles and is then sampled and converted in the AMU/ADC stage (see section 4.2). The final reported ADC value then varies linearly with the pulse arrival time. The relationship between time and the resulting ADC output voltage can be adjusted by programming the ramp slope and offset voltage remotely via ARCNet.

The energy signal is first put through a Variable Gain Amplifier (VGA). Each PMT channel has its own VGA and each of whose gains can be set remotely in the range $\times 4 - \times 12$ with 5-bit resolution. This allows the readout electronics to compensate, to within a few percent over its range, for gain variations among PMT's which share the same high voltage supply. Uniform response for the energy signal is useful in the performance of the trigger circuit (see section 4.3) and in general for maximizing the use of the ADC dynamic range for all channels.

The dynamic range of physics signals from the EMCal is quite large and the detector is expected to resolve energy deposits from 20 MeV up to 15–30 GeV with a noise contribution from the electronics of no more than 0.1% for large signals and 5 MeV for small signals. This range is impossible to cover with a single 12-bit ADC conversion. Thus the energy signal is converted twice with two different levels of amplification. The "low gain" signal is converted straight from the VGA and the "high gain" signal is converted separately after a second stage of $\times 16$ amplification. The results of both conversions are available when the digital output packet is assembled as discussed in section 4.2.

4.2 Conversion and Digital Processing

The voltage waveforms from the high- and low-gain energy stages and the TAC for each channel are sampled once per RHIC clock tick and stored in a series of Analog Memory Units (AMU's) as in several other PHENIX FEE systems [13]. Each waveform is sampled into a ring buffer of 64 AMU's, effectively preserving it for 64 RHIC clock ticks or about 7 microseconds, which easily covers the PHENIX LVL-1 (Level-1) trigger [13] latency of 40 RHIC clock ticks.

Upon receiving a LVL-1 Accept instruction the FEM identifies the energy and TAC AMU cells corresponding to the event. These AMU cells are then taken out of the ring buffer and converted in the ADC. The AMU rings and the ADC units are contained within another ASIC chip which was custom-designed for PHENIX and is used in several PHENIX readout systems. These ADC outputs are controlled, collected and reformatted by several Xilinx FPGA's, which are programmable remotely *in situ*. The formatted data "packet" for each event is then sent to a PHENIX Data Collection Module (DCM) [13] via GLINK across a PHENIX standard optical fiber.

4.3 EMCal Fast Trigger Function

At design luminosities, the rate of basic interactions in both A-A and p-p running in RHIC is too high for PHENIX to digitize and record all events. Since it is an explicit goal of PHENIX to use the full available luminosity to measure rare processes such as the production of heavy flavors and very high-energy secondaries, an ability to trigger on such processes is necessary. The EMCal FEE provides a fast-trigger function intended to signal the presence

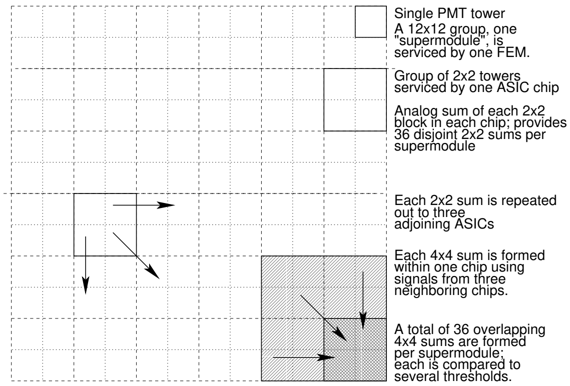

Fig. 17. Schematic of the EMCal fast trigger summing operation

of a high-energy shower in the EMCal detector. Electromagnetic showers with a large energy deposit (generally taken as above several GeV) are natural indicators of several kinds of interesting rare events, including high-energy photons and neutral mesons as well as high-energy electrons from heavy-flavor decays.

A traditional approach for a high-energy cluster trigger in a laterally segmented calorimeter is to make a fast analog sum of a group of towers and discriminate that sum against a threshold. In the simplest scheme each tower contributes to only one sum leaving the summed trigger groups disjointed. This arrangement has the drawback that the effective threshold is position dependent since showers which spread across more than one group need to have a much higher energy than those contained within one group.

The PHENIX EMCal fast trigger avoids this problem by summing over non-disjoint overlapping groups of towers. The design is illustrated in Fig. 17. Groups of 2×2 towers are served by one ASIC chip described above. Within each ASIC the four analog PMT signals are summed creating an array of disjoint 2×2 sums. To negate the influence of "hot" PMT's, each channel in each ASIC can be masked out of the sum individually by remote ARCNET control. Each ASIC relays copies of its signal generated by summing the current to three immediate neighbors. These are relayed between FEM's at supermodule boundaries making the trigger circuitry effectively seamless. Each ASIC also receives three signals from its neighbors and combines them with its own to form a 4×4 sum. The entire circuitry then produces 36 overlapping 4×4 sums in each FEM. Within each ASIC the 4×4 sum signal is compared to three separate thresholds, each remotely programmable, to provide extra flexibility for different physics processes.

5 Acknowledgements

This work was supported by the Department of Energy (U.S.A.).

References

[1] Article entitled “PHENIX Detector Overview” this volume.

[2] Article entitled “PHENIX Central Arm Tracking Detectors” this volume.

[3] E. Kistenev et al., Proc. of the 5th Internat. Conf. on Calorimetry in High Energy Physics, World Scientific (1994) 211.

[4] G. David et al., IEEE Trans. Nucl. Sci. 45, (1998).692

[5] G. David et al., IEEE Trans. Nucl. Sci. 45 (1998) 705.

[6] J.Stumer, private communication.

[7] R.Wigmans, private communication.

[8] G. David et al., IEEE Trans. Nucl. Sci. 47 (2000) 1982.

[9] WA98 Collaboration. CERN Report No. SPSLC 91-17 (1991).

[10] Article entitled “PHENIX Central Arm Particle I.D. Detectors” this volume.

[11] S. Neumaier et al., Nucl. Instr. and Meth. **A 360** (1995) 593.

[12] T. Peitzmann et al., Nucl. Instr. and Meth. **A 376** (1996) 368.

[13] Article entitled “PHENIX On-Line Systems” this volume.

[14] M.S. Emery et al., IEEE Trans. Nucl. Sci. 44 (1997) 374.